AIAA JOURNAL
Vol. 40, No. 10, October 2002

Experimental Study of the Three Dimensionality of Orthogonal Blade–Vortex Interaction

Tongguang Wang,* C. J. Doolan,† F. N. Coton,‡ and R. A. M. Galbraith§
University of Glasgow, Glasgow, Scotland G12 8QQ, United Kingdom

Wind-tunnel tests were conducted to investigate orthogonal vortex interaction with a stationary blade mimicking the main-rotor/tail-rotor interaction. High-quality experimental results with high-temporal resolution for the interaction have been obtained at different wind speeds and blade incidence angles. A vortex generator was specially designed for the experiment and produced stable trailing vortices. These were identified by hot-wire anemometry, with different vortical parameters for different speeds. When the measurement location is aligned with the vortex axis, pressure data reveal a suction peak on the upper blade surface and a pressure peak on the lower surface during the interaction. Significant dependence of the pressure on spanwise distance from the vortex indicates a strong three-dimensional interaction effect. For example, for spanwise positions above the core axis, a pressure pulse on the upper surface and a suction peak on the lower surface have been observed. It is shown that these differences can be attributed to the influence of the axial and tangential velocity components of the vortex. Pressure data for the blade at high incidence also show that the interaction can exacerbate and alleviate flow separation, depending on the spanwise position.

Nomenclature

C_n = normal force coefficient, $\oint C_{pu}\,\mathrm{d}\left(\frac{x}{c}\right)$
C_{n0} = normal force coefficient at $t = 0$
C_{pu} = unsteady pressure coefficient $(p/\frac{1}{2}\rho V^2)$
C_{p0} = pressure coefficient at $t = 0$
c = interacting blade chord
p = local static pressure
r_c = vortex core radius
T = airfoil thickness
t = sample time
V = freestream velocity
V_θ = vortex tangential velocity
v = vertical velocity
w = cross-stream velocity
w_0 = mean axial core velocity
x = chordwise distance measured from leading edge
y = ordinate of point on blade surface measured from chord line
z = spanwise distance from vortex axis
α = angle of incidence
Γ = circulation

Introduction

BLADE–VORTEX interaction (BVI) is a very important aerodynamic phenomenon, most often occurring in helicopter flight when the strong tip vortex trailing from a main rotor blade encounters another blade of the main rotor and/or the tail rotor. This kind of interaction can produce unwanted unsteady loading, noise, and vibration.[1] Much research has focused on the case of main rotor BVI where the vortex interacts with another main rotor blade, for example, Strauss et al.[2] and Masson et al.,[3] among many others. However, less is known about the orthogonal interaction of the main rotor vortex with a tail rotor blade. Understanding of the latter event is important to increase the performance and acceptance of future rotorcraft. In recent years, therefore, orthogonal BVI (OBVI) research has become of increased interest to aerodynamicists.

In forward flight, the tip vortex from a helicopter main rotor blade is ingested into the tail rotor disk and severed by the rotating blades. The trailing vortex can approach the tail rotor at various angles, but an important and limiting case is an orthogonal interaction. Previous research into the OBVI has included both mathematical and experimental studies. Analytical investigations have been conducted by Howe[4] and Marshall.[5] Computational studies[6–9] show that the vortex dynamics during cutting are controlled by the axial flow within the vortex core. If the axial flow is directed toward the cutting surface, the core bulges, and if the axial flow is away from the surface, the core thins (Fig. 1). This kind of vortex core distortion during the vortex chopping has been verified by flow visualizations.[8,10] The experimental studies also show the production of secondary vorticity and entrainment of the blade boundary layer into the core, which indicate the complexity of the OBVI mechanisms. Surface pressure and noise measurements of the orthogonal vortex interaction[11,12] show a difference in pressure measurements on either side of the cutting surface, which could possibly be due to an axial core component. However, the vortices produced in these experiments were representative of the wake of a hovering rotor or propeller rather than a helicopter in forward flight.

More recently, an experimental study of OBVI has been conducted in the Glasgow University 1.15×0.85 m low-speed wind tunnel both on unsteady pressure measurement and on flow visualization.[13–18] One of the unique features in the study is the use of a novel vortex generator. The method employed a one-bladed rotor rig, placed in the contraction of the wind tunnel, which pitched a symmetrical blade through a specific incidence profile as it rotated so as to generate a transverse vortex. That vortex was then convected through the wind tunnel and subsequently was cut by a blade mounted in the working section. The experiment gave invaluable results of OBVI both in surface pressure measurement and in flow visualization. However, the wandering amplitude of the vortex generated was estimated to be 19% of the interacting blade's chord or

Received 7 September 2001; revision received 15 February 2002; accepted for publication 18 April 2002.

*Postdoctoral Research Assistant, Department of Aerospace Engineering; currently Associate Professor, Department of Aerodynamics, Nanjing University of Aeronautics and Astronautics, Nanjing 210016, People's Republic of China.
†Postdoctoral Research Assistant, Department of Aerospace Engineering; currently Propulsion Systems Technology, Defence Science and Technology Organisation, Salisbury, South Australia 5108, Australia.
‡Reader, Department of Aerospace Engineering. Member AIAA.
§Professor, Department of Aerospace Engineering. Member AIAA.

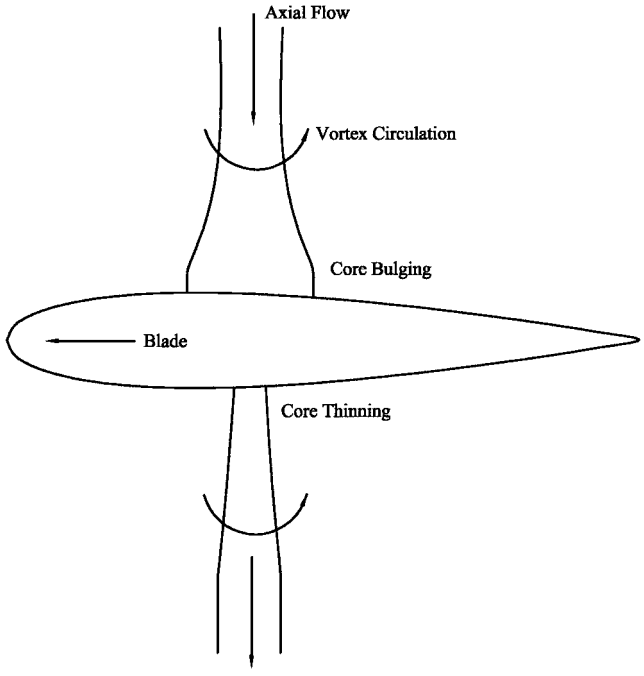

Fig. 1 Orthogonal vortex interaction.

29.5 mm; this was considered to be too large. It was, therefore, desirable in the second phase of the work to generate a more stable vortex to improve the experiment.

The second phase of the OBVI study was carried out in the Glasgow University 2.65 × 2.04 m Argyll wind tunnel, and the vortex produced by the new vortex generator proved to most satisfactory. In the present paper, the experimental results from this phase of the work are presented and discussed. First, velocity measurements of the three-dimensional vortex generated for the interaction are considered. These were obtained using hot-wire anemometry and confirmed the acceptability of the vortex generator. Second, an instrumented blade was then placed in the wind tunnel's working section to obtain surface pressures during the interaction for different wind speeds. The interacting blade was adjustable both vertically and in incidence. This permitted interactions at various vortex positions to be recorded, and also the effect of blade incidence to be examined.

Experiment

Experimental Facilities

The experiments were conducted in the Glasgow University 2.65 × 2.04 m Argyll low-speed wind tunnel. This is a closed-return facility with a maximum operating speed of 76 m/s. During testing, the freestream velocity and temperature were monitored continuously.

The new single-bladed vortex generator for use in the Argyll wind tunnel is larger than that used in the previous phases of the work.[19] It also required a refinement in technology and design that included a special hard-chromed cam plate together with a fully articulated rotor hub, which incorporates flap and lag hinges with a cantilevered flap spring and elastomeric lag dampers. It has a rotor of radius 1.6 m with a single rectangular planform blade of chord 0.16 m with a NACA 0015 cross section. The blade is rotated by a variable-frequency drive motor and is pitched to a maximum incidence of 10 deg using a spring-loaded pitch link running on a cylindrical cam configured such that the blade pitch varies smoothly in four equivalent (90-deg) phases of azimuth.[13–19]

Velocity measurements of the convecting tip vortex were made using a TSI IFA-300 constant temperature hot-wire anemometer system using DANTEC P61 cross-wire probes. The probes used 5-μm-diam plated tungsten wires with a length-to-diameter ratio of 250. The measuring volume of each probe was approximately 0.8 mm in diameter and 0.5 mm in height.

During interaction experiments, a NACA 0015 blade of chord 275 mm was mounted vertically in the path of the vortex (Fig. 2) at a location 4 m, or 14.55 blade chord lengths, downstream of the rotor rig axis. To avoid the worst of the turbulent wake from the vortex generator, the blade was placed on the right side 370 mm from the tunnel centerline, facing into the settling chamber. The two dimensionality of the flow at this position was established by hot-wire and blade pressure measurements with the vortex generator in situ but not operating. At this position, the vortex was predicted to collide nominally orthogonally with the blade using a numerical model comprising a free-wake analysis and panel method that simulated the vortex convection and wind-tunnel wall constraint.[19] The predictions from this model were validated by the hot-wire measurements in a manner similar to that described by Doolan et al.[16]

Table 1 Arrangement of transducers around blade section

Transducer no.	x/c, %	y/c, %
1	94.54	−1.0839
2	83.64	−2.7639
3	72.70	−4.2452
4	61.82	−5.5139
5	50.91	−6.5446
6	40.00	−7.2538
7	29.09	−7.4999
8	20.00	−7.1719
9	12.73	−6.3565
10	7.27	−5.1856
11	3.64	−3.8705
12	1.82	−2.8235
13	0.91	−2.0360
14	0	0
15	0.91	2.0360
16	1.82	2.8235
17	3.64	3.8705
18	7.27	5.1856
19	12.73	6.3565
20	20.00	7.1719
21	29.09	7.4999
22	40.00	7.2538
23	50.91	6.5446
24	61.82	5.5139
25	72.70	4.2452
26	83.64	2.7639
27	94.54	1.0839

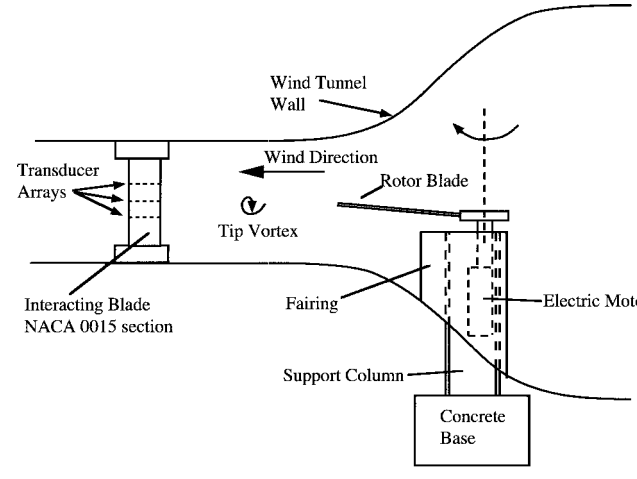

Fig. 2 Vortex generator and interacting blade in wind tunnel.

The blade was instrumented with the three chordal arrays of 27 miniature Sensym SCC05GSMT pressure transducers. These transducers have a frequency response of 10 kHz and were individually calibrated against a Druck DPI 610 pressure calibrator while wired to their own current sources. The separation distance between each array was 68.75 mm, and the positions of the transducers around the blade section are listed in Table 1. Additional transducers were placed between the chordal arrays to provide detail of spanwise loading distributions at six chordal locations. The transducers were connected to a surface orifice of 1-mm diam and

mounted as close as possible to the undersurface of the blade; however, because of the lack of space, three of the transducers were connected via small lengths of plastic tubing at the trailing-edge location. A computational analysis of this tubing arrangement indicated that no significant attenuation or phase shift would result. During testing, the blade could be set at different incidence values, and it could be moved vertically to allow the relative location of the chordal arrays with respect to the vortex core to be changed.

Test Program

The test program consisted of measuring the unsteady pressures during the OBVI. This was done for a variety of wind-tunnel speeds and blade settings. For the current tests, the freestream velocities used were 20, 30, 40 and 50 m/s, and the corresponding rotational speeds of the vortex generator were 168, 252, 336, and 420 rpm. These settings had been identified using the free-wake/panel method[19] to provide a clear, well-defined tip vortex structure in the working section. The blade angles of incidence ranged from −12 to 12 deg with a 2-deg increment.

Before these tests, a hot-wire survey was conducted to locate the vertical position of the vortex in the wind tunnel. The hot-wire probe was mounted on a computer-controlled traverse system 370 mm from the tunnel centerline at the location where the interacting blade would be placed. The probe was traversed vertically capturing the vortex velocity components. The height of the vortex center above the floor of the working section could be estimated from these measurement results.

The interacting blade could be moved vertically so that the chordal transducer arrays could be moved with respect to the interaction vortex. In the current program, five vertical positions were used, and so, with three arrays of transducers, the interactional data at a total of 15 blade sections were recorded for each speed and at each blade incidence setting. Table 2 lists the locations of the instrumented arrays with respect to the vortex center, where positive and negative values of z indicate that the array is above and below the vortex center (Fig. 3), respectively.

Table 2 Distances between instrumented blade section and vortex

Position no.	Vertical distance from instrumented section to vortex center z, mm	z/c
1	−108.75	−0.3954
2	−88.75	−0.3227
3	−68.75	−0.25
4	−48.75	−0.1772
5	−40	−0.1454
6	−28.75	−0.1045
7	−20	−0.0727
8	0	0
9	20	0.0727
10	28.75	0.1045
11	40	0.1454
12	48.75	0.1772
13	68.75	0.25
14	88.75	0.3227
15	108.75	0.3954

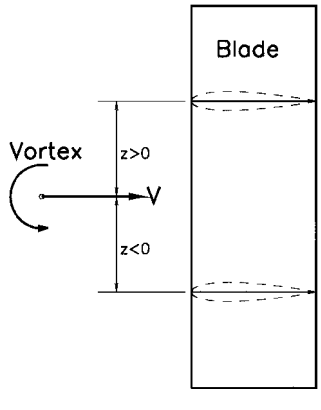

Fig. 3 Schematic showing relative position of blade section and vortex.

Data were acquired using the BE 256 data logger with a 50-kHz sampling rate in 16 blocks of 2000 samples each. The trigger timing was arranged so that each 2000 sample block contained a separate vortex interaction.

Experimental Errors

The data acquisition system and software has an automatic gain adjustment feature that allows measurements to be taken at the maximum resolution of the system. On the basis of previous experience with Kulite miniature transducers[3] and taking into account discretization and calibration factor errors, the uncertainty in the measured pressure coefficients is estimated to be 0.5%. Given this uncertainty in the pressure measurement, and accounting for the approximation of numerical integration, the uncertainty in the presented normal force coefficients is estimated to be 2.0%.

A source of uncertainty in the measurements was the vortex position. Once produced by the rotor rig, the vortex connects through the wind tunnel. Each successive vortex follows a slightly different path due to variations in local conditions on the rotor blade and freestream turbulence levels. When a numerical procedure[16] is used to analyze the hot-wire measurements, the wandering amplitude of the vortices has been estimated to be 5 mm or 1.8% of the interacting blade chord. This is much smaller than the previous amplitude of vortex wandering produced by the small rotor rig in the first phase of the investigation.[15]

Results and Discussion

Vortex Parameters

The vortex was expected to interact with the instrumented blade orthogonally. The height of vortex core passage was determined using two criteria. These consisted of the height where the maximum vertical velocity was measured (a measure of the vortex tangential velocity) and also where the measured freestream component changed from a negative reinforcement (indicating that the vortex passed beneath the probe) to a positive reinforcement (vortex passage above the probe). Vortex wander usually showed both positive and negative reinforcements in successive vortices at the approximate vortex passage height. When an estimation method developed by Doolan et al.[16] was used, the vortex passage height in these tests was located to within 5 mm, indicating significantly lower wandering than the 29.5 mm (Ref. 16) measured in the test using the small-scale vortex generator rig. This provided a basis on which more reliable interaction information could be obtained. The vortex passage heights at different wind speeds and the corresponding vortex generator speeds are given in Table 3.

Figure 4 shows the measured vertical velocity component at the vortex passage height for different freestream velocities. For $V = 20$ m/s, the data show a characteristic vortex signal of an induced velocity field around a viscous core region. Also, the peak velocity signal is higher on the inboard, or downstream side, of the vortex. This is due to the curvature of the vortex causing a self-induced increase in velocity magnitude. Strong vortex signals are again noticed at $V = 30$ and 40 m/s. However, a periodic disturbance between each vortex can be identified. This disturbance becomes dominant at 50 m/s freestream and takes the form of another convecting vortex rotating in the opposite sense. The strength of this

Table 3 Summary of vortex parameters

	V, m/s			
Parameter	20	30	40	50
Rotor speed, rpm	168	252	336	420
Vortex height, mm	980	960	920	900
r_c, mm	74.18 ± 16.35	84.83 ± 33.31	76.30 ± 10.24	90.30 ± 49.32
Maximum V_θ, m/s	2.77 ± 0.35	3.20 ± 0.45	3.17 ± 0.38	1.72 ± 0.41
w_0, m/s	1.62 ± 0.23	1.27 ± 0.23	1.91 ± 0.25	2.20 ± 0.20
Γ, m^2/s	0.90 ± 0.26	1.26 ± 0.41	1.26 ± 0.25	0.77 ± 0.27
T/r_c	0.556	0.486	0.541	0.457
$2\pi r_c V/\Gamma$	10.36	12.69	15.22	36.84
$2\pi r_c w_0/\Gamma$	0.84	0.54	0.73	1.62

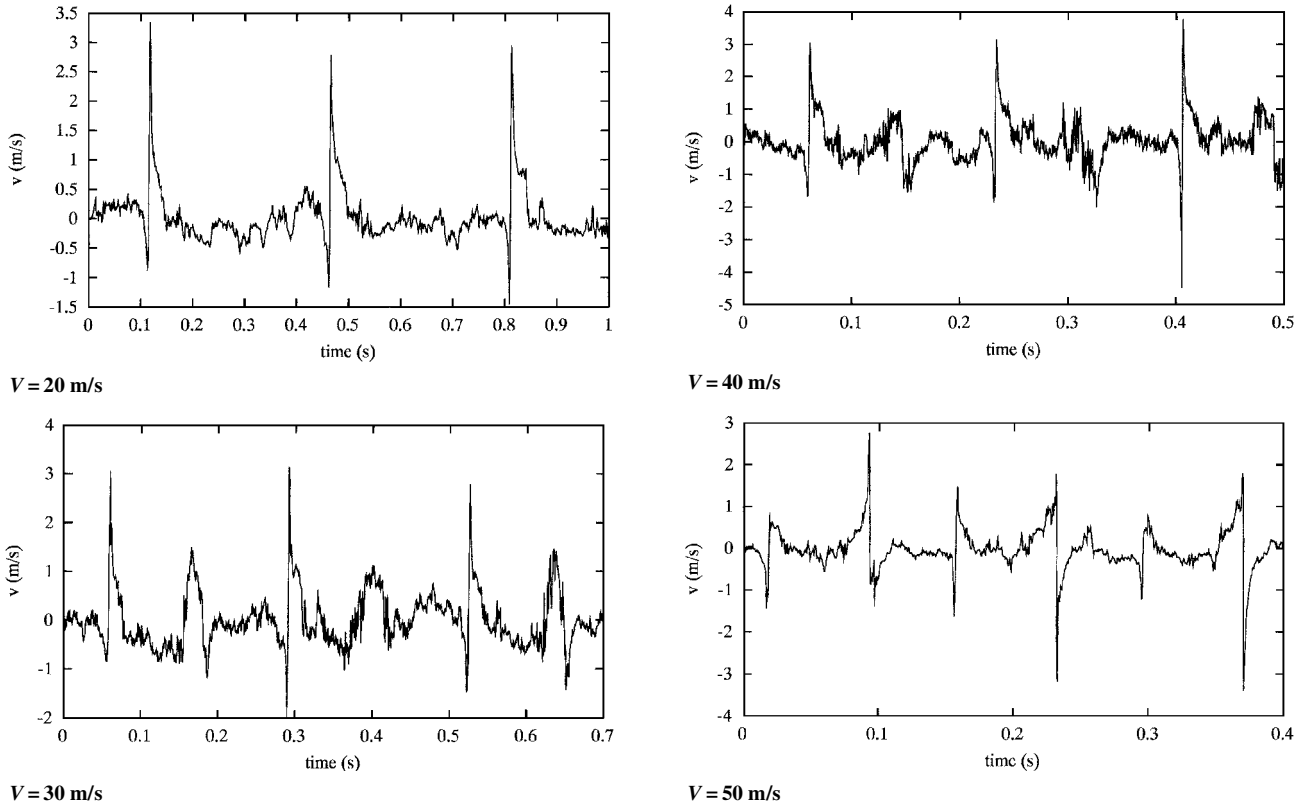

Fig. 4 Vertical velocity record at vortex passage height.

counter-rotating vortex is significantly greater than the primary vortex that the generator was designed to produce. These two vortices are separated by a time period of about 0.07 s, whereas the time period of the pressure data acquisition was 0.04 s around the primary vortex. This counter-rotating vortex, therefore, had little influence on the collected data.

The counter-rotating vortex may be attributed to the flapping motion of the blade. At $V = 50$ m/s, this motion could significantly increase the effective incidence of the blade while it is pointing into the settling chamber. It may also cause a decrease in effective incidence while the blade is pointing toward the working section. Only through a dynamic study of the rotor/hub combination could an understanding of this event be known. However, the very periodic nature of the disturbance may suggest that its origin exists at the blade tip.

By the rotation of the probe through 90 deg, the cross-stream velocity component can be measured. When the probe is placed at the vortex passage height, the axial component of the vortex core flow is acquired. Figure 5 shows the measured cross-stream component of the core flow for $V = 20$ and 30 m/s. In each case, an axial core velocity was measured in the direction of rotor rotation. The magnitude of the core component is of the same order as the peak tangential velocity component. This is a similar result to the velocity measurements taken with the small-scale rig.[13]

A summary of the vortex parameters can be found in Table 3. The information for the core radius r_c, maximum vortex tangential velocity V_θ, mean axial velocity w_0 within the core, and vortex strength Γ is presented as a mean value and with a tolerance that represents the standard deviation over 10 vortex measurements. The other values for the thickness parameter T/r_c, impact parameter $2\pi r_c V/\Gamma$, and axial flow parameter $2\pi r_c w_0 V/\Gamma$ are calculated using their corresponding mean values. Note that the high tolerance on some values may not indicate such large variations in successive vortex structure. Hot-wire probe interference can affect the information, particularly core size.[16]

Three dimensionless parameters have been identified by Marshall and Krishnamoorthy[8] as quantities that indicate the severity of the physical response to the vortex cut: They are the impact parameter $2\pi r_c V/\Gamma$, which represents the ratio of the relative impact velocity

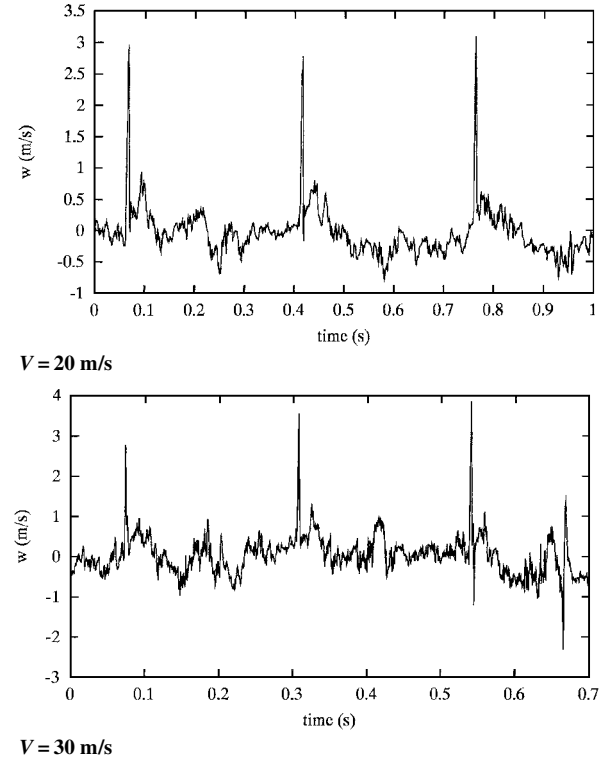

Fig. 5 Cross-stream velocity record at vortex passage height.

of the vortex blade to the maximum vortex tangential velocity, the thickness parameter T/r_c, which is the ratio of the blade maximum thickness to the vortex core radius, and the axial flow parameter $2\pi r_c w_0 V/\Gamma$, which is the ratio of the mean axial velocity within the core to the maximum vortex tangential velocity. In the present case, the relatively large core size results in very high values of $2\pi r_c V/\Gamma$ and small values of T/r_c, which implies that the vortex swirling motion causes no boundary-layer separation from the blade before

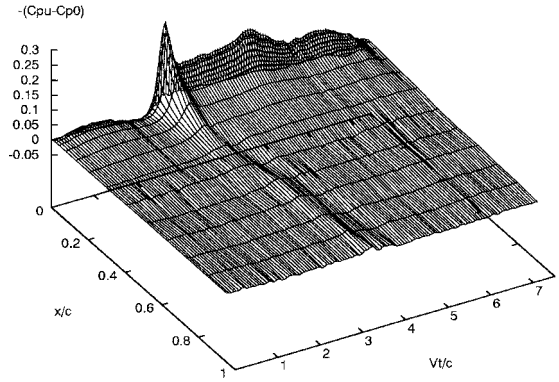

a) Upper surface at vortex height ($z/c = 0$)

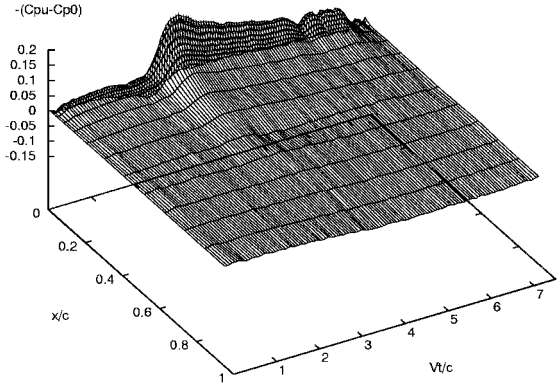

b) Upper surface below vortex height ($z/c = -0.3227$)

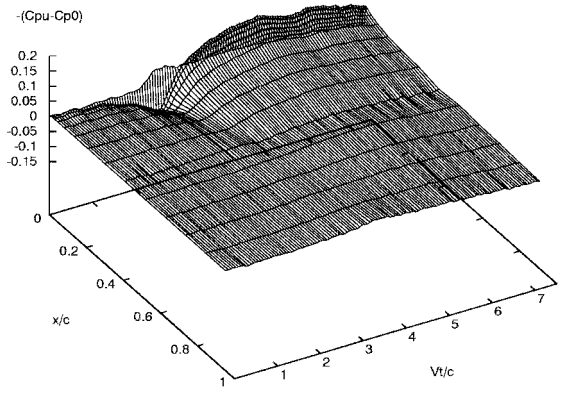

c) Upper surface above vortex height ($z/c = 0.3227$)

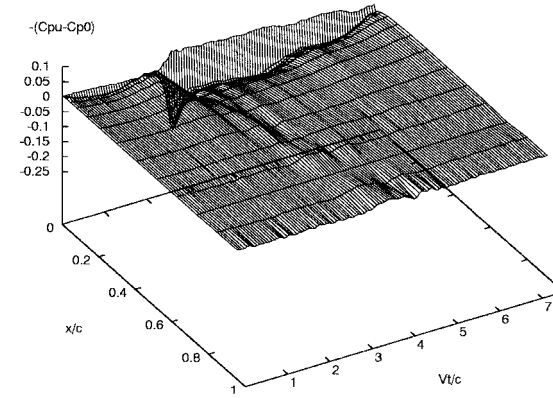

d) Lower surface at vortex height ($z/c = 0$)

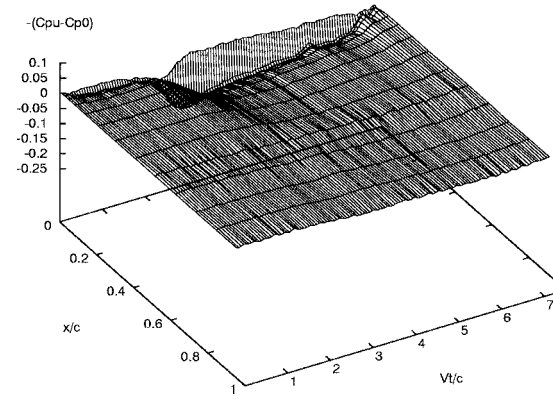

e) Lower surface below vortex height ($z/c = -0.3227$)

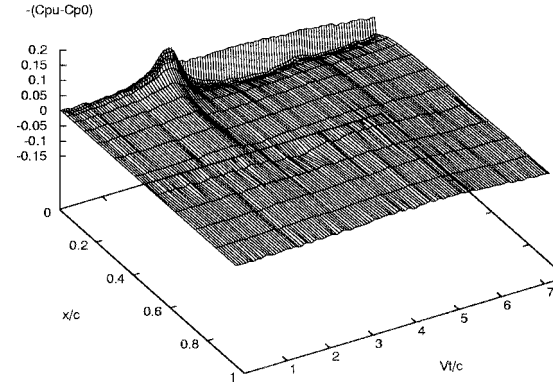

f) Lower surface above vortex height ($z/c = 0.3227$)

Fig. 6 Pressure measurement on airfoil surface for $V = 50$ m/s and $\alpha = 0$ deg.

the vortex impingement. This kind of weak interaction, a dominant feature during main rotor/tail rotor interaction for a helicopter in forward flight,[10] is also accompanied by little vortex deformation before the vortex collision with the leading edge.[6]

The value of the axial flow parameter determines the vortex response during vortex cutting. It has been shown with an assumption of uniform axial velocity and vorticity that the flow is supercritical for $2\pi r_c w_0/\Gamma > \sqrt{2}/2$ and subcritical for the axial flow parameter less than this value.[20] It can be seen from Table 3 that, depending on the freestream velocity and vortex generator speed, the experiment involved both supercritical and subcritical flows. The subcritical flow implies both upstream- and downstream-propagating waves of small amplitude. For the supercritical flow, only downstream-propagating waves of small amplitude can be supported in the core, a jetlike flow impacts on the cutting surface of the blade, and a thinning of the vortex core occurs on the other side of the blade.

The large vortex core and low peak swirling velocity obtained in this study make the interactions weak. They will, however, be beneficial for any future laser-based flow measurement such as particle image velocimetry because the lower peak velocity and larger core will facilitate seeding within the core region.

Interaction with an Unloaded Blade

Doolan et al.[15] described the unsteady surface pressure variations experienced by a blade set at zero incidence during OBVI. Although the present tests were conducted at higher wind-tunnel velocities than those in Ref. 15, similar, although not identical, trends were observed. Figure 6 shows the temporal variation of the upper and lower surface pressure distributions at three measurement positions relative to the vortex core for a wind speed of 50 m/s. The lower surface of the blade is defined as the cutting surface toward which the axial flow is directed and the upper surface as the side from which the axial flow is away. The directions of positive and negative blade incidence are also defined on this basis. In Fig. 6, the initial value of the pressure C_{p0} at time $t = 0$, has been removed from the unsteady data C_{pu} for clarity. To increase the clarity of Figs. 6 further, only every 16th data sample is presented. If the vortex deformation is negligible before interaction, the pressure distribution C_{p0} at the sample time $t = 0$ can be regarded as the clean pressure on the blade surface in a flowfield with vortex induction. Therefore, the value of $-(C_{pu} - C_{p0})$ on the vertical axis represents the net contribution of the interaction to the surface pressure. The other two axes in the plot denote the chordal position x/c and the nondimensional time Vt/c, respectively.

At $z/c = 0$, the upper surface data in Fig. 6a show a strong suction peak at the leading edge when the vortex encounters the blade. The subsequent passage of the vortex over the surface produces a suction ridge that abates toward the trailing edge. Meanwhile, the interaction retains its influence on the upper surface loading in the form of increased suction in the leading-edge region. In fact, the vortex has passed downstream by several chord lengths before the pressure returns to its clean value C_{p0}.

For the lower surface (Fig. 6d), an increase in pressure occurs just downstream of the leading edge when the vortex collides with the blade. With the passage of the vortex over the chord, this impacting pressure decreases, and eventually the pressure ridge transforms into a slight suction ridge. The magnitude of the pressure and suction ridges on the lower surface is less than that of the suction ridge on the upper surface. Note that, for all lower surface plots in this paper, the leading-edge pressure record is presented for completeness.

The aspects of the pressure response to the orthogonal vortex cutting for both upper and lower surfaces identified earlier have been observed previously for the small-scale vortex generator case.[15] As in the previous study, before the encounter of the vortex core with the blade ($Vt/c \approx 0 \sim 1$), the pressure, even in the leading edge, deviates little from the initial value C_{p0}, attesting again that there is little vortex deformation and little interactional effect before the blade–vortex collision for the weak interaction case. The current results do, however, show a generally lower level of response in terms of both peak and ridge values. This may be attributed to the higher value of the impact parameter in this case, producing a generally weaker interaction. Also, in Ref. 15, the unsteady response to the interaction is rapid, short lived, and localized, whereas, in this case, the duration of the interaction is much longer. One likely reason for this is the much larger ratio of the vortex core radius to airfoil chord in this case (0.328) compared with that of Ref. 15 (0.065).

When the measurement location is below the vortex ($z/c < 0$), the upper surface interaction is characterized by enhanced suction in the leading-edge region that diminishes with distance from the vortex axis. According to the so-called tornado effect of Hagen and Kurosaka,[21] the vortex cutting results in a pressure gradient, which pumps fluid away from the upper surface through the (distorted) vortex core. Figure 6b shows the pressure variation for the case when the transducer array just coincides with the edge of the vortex core. At this location, the rise in suction during the interaction is less dramatic than when the measurement array is aligned with the vortex core. There is also no evidence of the sustained suction ridge that extended to the trailing edge in the previous case. In fact, this ridge was only apparent at measurement locations that lay within one-half of the core radius from the vortex axis. Again, this result differs from that observed in Ref. 15, where the suction ridge was apparent when the measurement station was as much as two core radii below the vortex axis. This may again be attributed to the higher impact parameter in the present case producing a weaker interaction.

The corresponding lower surface pressure response is presented in Fig. 6e. At this location, and for all measurement locations below the vortex axis, a pressure peak is evident in the leading-edge region. Unlike the response observed when the measurement location was on the vortex axis, there is little evidence of the effect of the vortex downstream of the leading edge. Again, presumably as a consequence of the higher impact parameter in this case, this result differs markedly from Ref. 15, where a strong suction ridge was observed on aft portions of the chord on a measurement section two core radii below the vortex axis.

When the vortex passes below the measurement section ($z/c > 0$), the magnitude of the upper surface suction peak at the leading edge decreases with increased vertical distance between the vortex and the measurement section in a similar manner to that described earlier. However, significant differences between the responses at measurement locations above and below the vortex become apparent as the distance between the measurement location and the vortex axis increases and the dominance of the axial core flow diminishes. Most noticeably (Fig. 6c) in the leading-edge region, a pressure trough forms and becomes more significant with increasing z. Note that this trough was not observed by Doolan et al.[15] This discrepancy may be attributed to two aspects of the tests. First, as already mentioned, the size of the vortex core relative to the blade chord in the current tests is much larger than in the first phase. This may result in reduced localized coupling between axial and rotational flow influences from the vortex. Second, the vortex wander was much greater in Ref. 15, which increased the uncertainty in the measured values.

At first glance, this pressure trough on the upper surface seems contradictory to the tornado effect of Hagen and Kurosaka.[21] In fact, the flowfield over the blade section for $z > 0$ is different from that for $z < 0$. As the vortex approaches the blade, the vortex induces a negative reinforcement in streamwise velocity for $z > 0$ and a positive reinforcement for $z < 0$ (Fig. 3). During vortex cutting, the distorted primary vortex and shed secondary vortex[22] produce complicated but distinct flowfields for different vortex passages relative to the blade section under consideration. These different vortex-induced flows can mix with the boundary layer over the blade and pump fluid away from the boundary layer on one side of the section and ingest fluid into the boundary layer on the other side. These different flow patterns at the different spanwise positions have been identified by Early et al.[18] in a flow visualization study.

For measurement locations where $z/c > 0$, the lower surface pressure response close to the vortex axis is similar to that shown in Fig. 6d. With increasing distance between the measurement location and the vortex axis, the leading-edge pressure peak and suction ridge, noted in Fig. 6d, gradually diminish, and a suction peak forms in the leading edge region (Fig. 6f). This suction peak seems to reach its maximum value when the blade section is situated at the vortex core edge where the maximum swirling velocity is obtained. Note that this suction peak was not observed in Ref. 15. This may also be indicative of reduced localized coupling between the axial and rotational flows in the vortex in the present case.

Integrating the pressure distribution along the surface yields the forces and pitching moment on the airfoil at a given measurement location. Figure 7 illustrates the difference between the instantaneous normal force coefficient C_n and the initial value C_{n0}, at time $t = 0$, during the interaction for $V = 50$ m/s and $\alpha = 0$ at five measurement positions relative to the vortex axis. Generally, the normal force coefficient changes little before nondimensional time $Vt/c = 1.5$, due to minimal deformation of the vortex because of the low ratio of the airfoil thickness to the core size, T/r_c. A small decrease in the normal force then follows before it rises abruptly. This initial decrease can be related to the pressure traces presented in the earlier figures. For example, if the C_n response at $z/c = 0$ is referenced to Fig. 6a, it may be observed that there is a localized increase in pressure at the upper surface leading edge just before to the rapid rise in leading-edge suction. This occurs at a nondimensional time of approximately 2 and is accompanied by a corresponding rise in suction on the lower surface (Fig. 6d). These two effects combine to produce the drop in normal force coefficient identified in Fig. 7. This drop is followed by an abrupt rise between $Vt/c \approx 2$ and 3, which is caused by the formation of the sharp suction and pressure peaks on the upper and low surfaces, respectively. After reaching its maximum value, the normal force behavior becomes very dependent on the relative position of the measurement location with respect to the vortex. For $z/c = 0$ and -0.0727, the normal force decreases as the vortex passes over the chord and the pressure peak on the lower surface transforms into a suction ridge. At the lowest measurement position, $z/c = -0.3954$, the drop in C_n is much more gradual, presumably because this location lies outside the vortex core and the tangential component of the vortex flow provides a positive reinforcement of the local dynamic pressure throughout the interaction. When the measurement location is above the vortex, the rise in C_n is less significant than in the other cases. Indeed, the C_n continues to rise even after the vortex has passed the trailing edge, albeit at a reduced rate. It is likely that this is indicative of the amelioration of the negative induced velocities produced by the sense of rotation of the vortex at measurement locations above the vortex centerline. After the vortex moves farther downstream from the trailing edge, the values of C_n for different positions tend to converge on a stable value and decrease gradually with time.

As expected, the rate of change in C_n is at its maximum when the measurement section aligns with the vortex passage height and the rate decreases with increased vertical distance between the

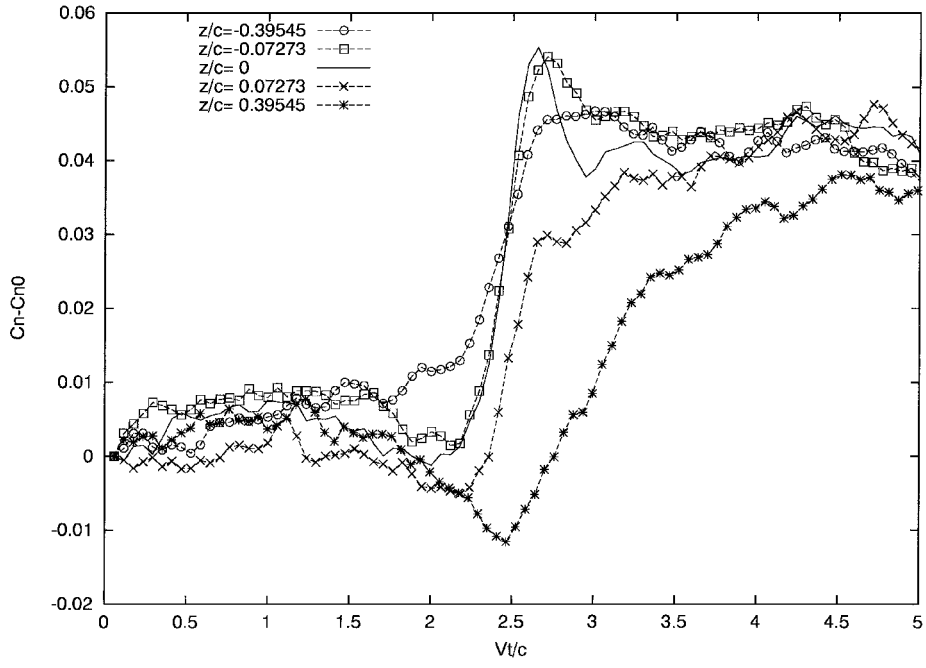

Fig. 7 Variation of normal force coefficient during interaction at $V = 50$ m/s and $\alpha = 0$ deg.

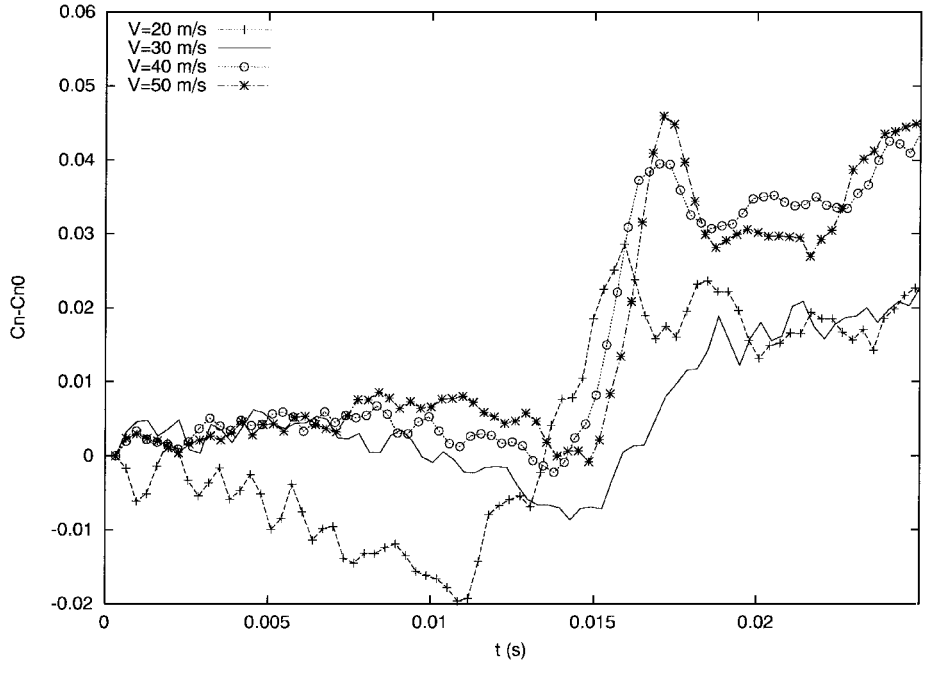

Fig. 8 Variation of normal force coefficient during interaction at $\alpha = 6$ deg and $z/c = 0$ for different wind speeds.

measurement section and the vortex. For $z > 0$, where the streamwise velocity along the chord is lower than for $z < 0$ because of the vortex induction, the effect of the interaction on the normal force is more gradual and less severe.

Interaction with Loaded Blade

Surface pressure measurements, and integrated force coefficients, for the orthogonal interaction of a vortex with a blade at incidence have been previously described by Doolan et al.[13] Because the unsteady pressure responses observed during the present series of tests are broadly similar to those described in Ref. 13, they will not be described in detail here. Rather, this discussion will focus on aspects of the present results that differ from those presented previously.

Figure 8 shows the variation with time of the interactional contribution to the normal force coefficient for different freestream velocities for the $\alpha = 6$ deg and $z/c = 0$ case. One interesting feature in Fig. 8 is that the impulsive increment in $(C_n - C_{n0})$ in the case of $V = 30$ m/s is much less than in the other three cases for which the normal force increments exhibit considerable similarity. The Reynolds number will inevitably play a role in the normal force variation with velocity, and this may be one of the reasons for the differences in $(C_n - C_{n0})$ for the various cases. However, it is unlikely to be the only reason because it has already been shown that the physical behavior during vortex cutting is strongly influenced by specific vortex parameters. Note that the only case for which the axial flow parameter (Table 3) is subcritical is the $V = 30$ m/s case, whereas the flow around the blade on impingement at the other three velocities, and in the cases previously reported by Doolan et al.,[15] is supercritical.[8,20] For the subcritical flow, the pressure waves propagate both upstream and downstream[8] resulting in a more moderate vortex cutting response. Marshall and Krishnamoorthy[8] provided a theoretical estimate of the normal force coefficient response during vortex cutting for subcritical flows. They noted that the response is characterized by a reduction in normal force in the early stages

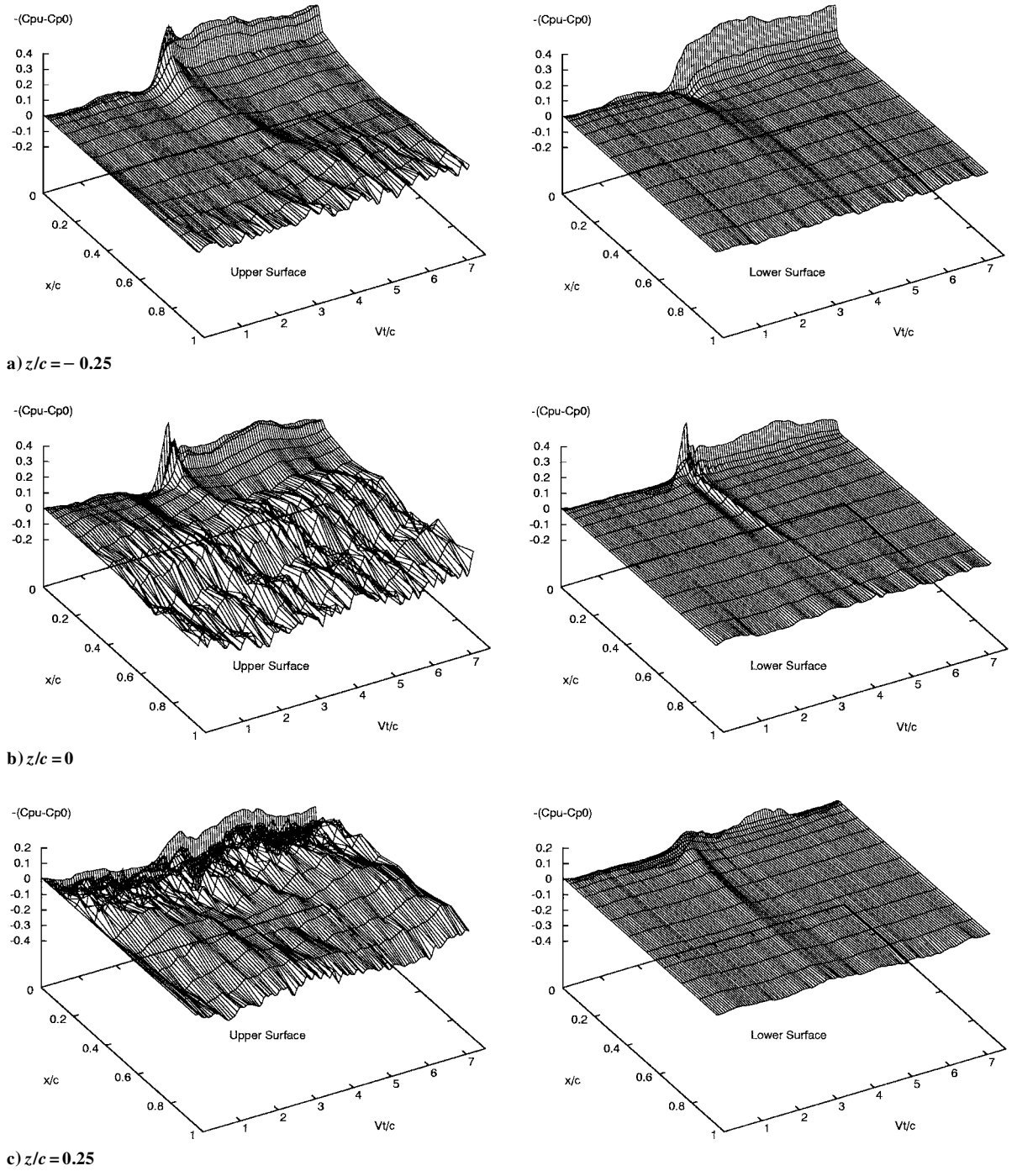

Fig. 9 Surface pressures measured at $\alpha = 12$ deg for $V = 50$ m/s.

of the interaction followed by a monotonic rise toward an asymptotic value. This description is in general agreement with the result presented in Fig. 8 at $V = 30$ m/s.

The effect of the interaction on flow separation was not examined in previous studies, primarily because of the low test Reynolds numbers. To examine this in the present study, the blade was set to 12 deg in both positive and negative senses. The highest flow speed, $V = 50$ m/s, corresponds to a chord Reynolds number of 9.45×10^5 at which, without vortex interaction, the blade should exhibit some degree of separation from the upper surface at $\alpha = 12$ deg and from the lower surface at $\alpha = -12$ deg, respectively.[23]

Figure 9 shows the pressure distribution on the airfoil section at three measurement positions relative to the vortex axis, for $V = 50$ m/s and $\alpha = 12$ deg. For the case of $z/c = 0$, the unsteadiness in the pressure histories indicates that significantly separated flow exists over approximately 70% of the chord on the upper surface. Understandably, the axial core flow away from the surface produces increased suction at the leading edge, exacerbating the adverse pressure gradient and, thus, promoting separation.

When the vortex passes above the measurement station, $z/c = -0.25$, the severity of separation is eased. The entire reason for this is unclear at present, but, in addition to the airfoil boundary-layer interaction with the offset vortex, the reinforcement in streamwise velocity due to the vortex tangential component may thin the boundary layer, delaying flow separation until the region of the trailing edge. On the other hand, when the vortex passes below the instrumented section, $z/c = 0.25$, the reduction in streamwise velocity together with the interaction causes severe separation in the leading-edge region on the upper surface. At this section, the leading-edge suction peak is effectively destroyed, and the blade section is fully stalled. As may be expected, the flow over the lower surface at $\alpha = 12$ deg shows no obvious separation for all three cases.

Given that the interacting blade has a symmetrical NACA 0015 section, the flow pattern over the lower surface at $\alpha = -12$ deg

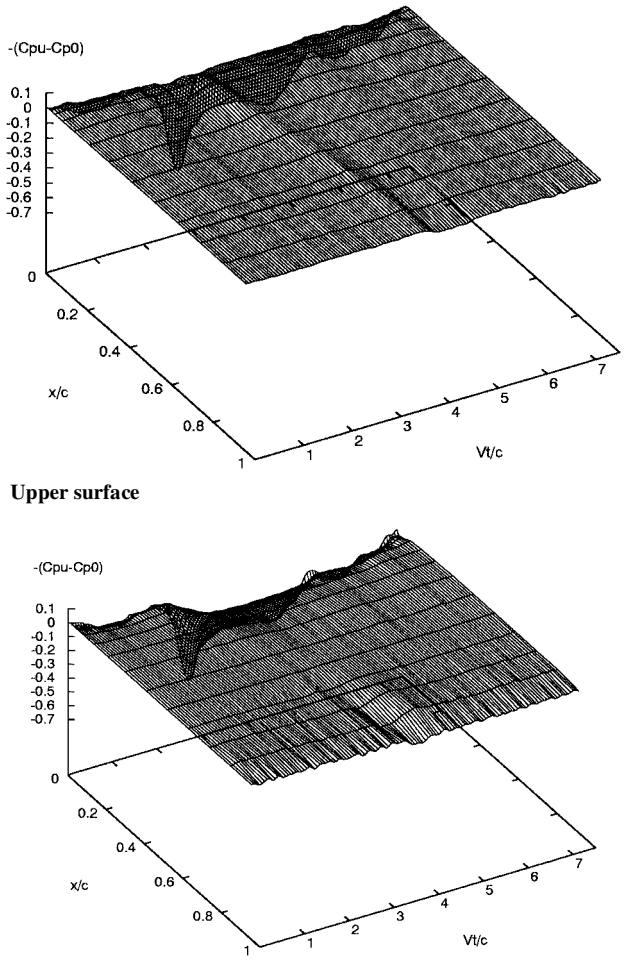

Fig. 10 Surface pressures measured at $\alpha = -12$ deg for $V = 50$ m/s and $z/c = 0$.

may be expected to be the same as that over the upper surface at $\alpha = 12$ deg without vortex interaction. In the OBVI case, this flow symmetry no longer exists. Figure 10 shows that the flow over the lower surface at $\alpha = -12$ deg primarily remains attached during the vortex cutting whereas, as discussed earlier, there is significant separation on the upper surface at $\alpha = 12$ deg for the same wind speed (Fig. 9b). This asymmetry arises from the impact of the axial core flow, which, at $\alpha = -12$ deg, energizes the lower surface boundary layer, diminishing flow separation. Conversely, when $\alpha = 12$ deg, the core flow is away from the upper surface and, as shown earlier, would be expected to enhance the adverse pressure gradient aft of the leading edge.

Conclusions

A vortex generator consisting of a single blade of 1.6-m radius has been designed for the purpose of an OBVI study in a 2.65×2.04 m low-speed wind tunnel. Velocity measurements using hot-wire anemometry showed that well-defined, three-dimensional vortices with different strengths and core sizes were produced and that the vortex wandering range was within 5 mm. The high impacting parameter obtained implied a weak vortex interaction.

A series of wind-tunnel tests were conducted, which investigated the orthogonal vortex interaction with an instrumented stationary blade. High-quality experimental results with high-temporal resolution for the interaction have been obtained at different wind speeds and various blade incidence angles for a number of vortex passage positions relative to the blade section where the pressure was recorded.

Pressure data at different spanwise positions relative to the vortex axis were acquired and exhibited strong three-dimensional variations with time and distance from the vortex axis. The suction peak on the upper surface and the pressure peak on the lower surface decreased with increasing spanwise distance from the vortex axis. For spanwise positions below the vortex axis, the pressure results were similar to those at the vortex passage height, but the interactional effects diminished as the distance increased. However, for spanwise positions above the core axis, a pressure pulse and a suction peak in the leading-edge region on the upper and lower surfaces, respectively, became apparent when the distance increased. Several aspects of this behavior differ from previous measurements of OBVI made in a smaller test facility.

Integrated normal force data showed a rapid rise as the vortex impacted with the leading edge. The rate of change of normal force decreased as the spanwise measurement distance to the vortex was increased. The normal force increment also exhibited a dependency on whether the flow was sub- or supercritical in terms of the vortex axial flow parameter.

The results of interactions with the blade at high incidence showed that the interaction could both exacerbate and diminish flow separation, depending on the spanwise position. On the cutting surface toward which the core flow was directed, the separation was diminished.

Acknowledgments

This work was funded by the Engineering and Physical Sciences Research Council, the Defence Evaluation and Research Agency, Farnborough, and GKN–Westland Helicopters, Ltd., under Grant Number GR/L 58231. The authors would also like to thank the technical staff of the Department of Aerospace Engineering for their valuable assistance.

References

[1]Sheridan, P. F., and Smith, R. P., "Interactional Aerodynamics—A New Challenge to Helicopter Technology," *Journal of the American Helicopter Society*, Vol. 25, No. 1, 1980, pp. 3–21.

[2]Straus, J., Renzoni, P., and Mayle, R., "Airfoil Pressure Measurements During a Blade–Vortex Interaction and Comparison with Theory," *AIAA Journal*, Vol. 28, No. 2, 1990, pp. 222–228.

[3]Masson, C. A., Green, R. B., Galbraith, R. A. M., and Coton, F. N., "Experimental Investigation of a Loaded Rotor Blade's Interaction with a Single Vortex," *Aeronautical Journal*, Vol. 102, No. 1018, 1998, pp. 451–457.

[4]Howe, M., "On Unsteady Surface Forces, and Sound Produced by the Normal Chopping of a Rectilinear Vortex," *Journal of Fluid Mechanics*, Vol. 206, 1989, pp. 131–153.

[5]Marshall, J. S., "Vortex Cutting by a Blade, Part 1: General Theory and a Simple Solution," *AIAA Journal*, Vol. 32, No. 6, 1994, pp. 1145–1150.

[6]Marshall, J. S., and Yalamanchili, R., "Vortex Cutting by a Blade, Part 2: Computations of Vortex Response," *AIAA Journal*, Vol. 32, No. 7, 1994, pp. 1428–1436.

[7]Marshall, J. S., and Grant, J. R., "Penetration of a Blade into a Vortex Core: Vorticity Response and Unsteady Blade Forces," *Journal of Fluid Mechanics*, Vol. 306, 1996, pp. 83–109.

[8]Marshall, J. S., and Krishnamoorthy, S., "On the Instantaneous Cutting of a Columnar Vortex with Non-Zero Axial Flow," *Journal of Fluid Mechanics*, Vol. 351, 1997, pp. 41–74.

[9]Lee, J. A., Burggraf, O. R., and Conlisk, A. T., "On the Impulsive Blocking of a Vortex Jet," *Journal of Fluid Mechanics*, Vol. 369, 1998, pp. 301–331.

[10]Krishnamoorthy, S., and Marshall, J. S., "Three-Dimensional Blade Vortex Interaction in the Strong Vortex Regime," *Physics of Fluids*, Vol. 10, No. 11, 1998, pp. 2828–2845.

[11]Ahmadi, A., "Experimental Investigation of Blade–Vortex Interaction at Normal Incidence," *AIAA Journal*, Vol. 23, No. 1, 1986, pp. 47–55.

[12]Johnston, R. T., and Sullivan, J. P., "Unsteady Wing Surface Pressures in the Wake of Propeller," AIAA Paper 92-0277, 1992.

[13]Doolan, C. J., Coton, F. N., and Galbraith, R. A. McD., "Surface Pressure Measurements of the Orthogonal Vortex Interaction," *AIAA Journal*, Vol. 39, No. 1, 2001, pp. 88–95.

[14]Doolan, C. J., Green, R. B., Coton, F. N., and Galbraith, R. A. McD., "The Orthogonal Blade–Vortex Interaction Experimental Programme at the University of Glasgow," *26th European Rotorcraft Forum*, The Hague, 2000, pp. 103.1–103.12.

[15]Doolan, C. J., Coton, F. N., and Galbraith, R. A. McD., "Three-Dimensional Vortex Interactions with a Stationary Blade," *Aeronautical Journal*, Vol. 103, No. 1030, 1999, pp. 579–587.

[16]Doolan, C. J., Coton, F. N., and Galbraith, R. A. McD., "Measurements of Three-Dimensional Vortices Using a Hot-Wire Anemometer," AIAA Paper 99-3810, 1999.

[17]Green, R. B., Doolan, C. J., and Cannon, R. M., "Measurements of the Orthogonal Blade–Vortex Interaction Using a Particle Image Velocimetry Technique," *Experiments in Fluids*, Vol. 29, No. 4, 2000, pp. 369–379.

[18]Early, J. M., Green, R. B., and Coton, F. N., "Flow Visualisation of the Orthogonal Blade–Vortex Interaction Using Particle Image Velocimetry," *Aeronautical Journal*, Vol. 106, No. 1057, 2001, pp. 137–145.

[19]Copland, C. M., "The Generation of Transverse and Longitudinal Vortices in Low Speed Wind Tunnels," Ph.D. Dissertation, Dept. of Aerospace Engineering, Univ. of Glasgow, Glasgow, Scotland, U.K., 1997.

[20]Lundgren, T. S., and Ashurst, W. T., "Area-Varying Waves on Curved Vortex Tubes with Application to Vortex Breakdown," *Journal of Fluid Mechanics*, Vol. 200, 1989, pp. 283–307.

[21]Hagen, J. P., and Kurosaka, M., "Corewise Cross-Flow Transport in Hairpin Vortices—The "Tornado Effect," *Physics of Fluids*, Vol. A5, No. 12, 1993, pp. 3167–3174.

[22]Kaykayoglu, R., and Rockwell, D., "Vortices Incident Upon a Leading Edge: Instantaneous Pressure Fields," *Journal of Fluid Mechanics*, Vol. 156, 1985, pp. 439–461.

[23]Abbott, I. H., and von Doenhoff, A. E., *Theory of Wing Sections*, Dover, New York, 1959, Chap. 7.

W. J. Devenport
Associate Editor